Article

Investigation of the Wettability Properties of Different Textured Lead/Lead-Free Bronze Coatings

Amani Khaskhoussi , **Giacomo Risitano** , **Luigi Calabrese** and **Danilo D'Andrea** *

Department of Engineering, University of Messina, Contrada di Dio, 98166 Messina, Italy;
amani.khaskhoussi@unime.it (A.K.); grisitano@unime.it (G.R.); luigi.calabrese@unime.it (L.C.)
* Correspondence: dandread@unime.it; Tel.: +39-39-3020-9246

Abstract: Hydraulic components are often subjected to sliding contacts under starved or mixed lubrication. The condition of starved lubrication occurs during the start-up phase of the hydraulic machines or at low working temperature, causing friction and wear of components such as the cylinder block or the valve plate. The aim of this paper was to evaluate the hydrophobicity and oleophilic behavior of lead/lead-free bronze coatings under different texture conditions obtained by varying the diameter and the density of the dimples. The wettability tests were performed using sessile drop tests with oil and water liquids. The dimple parameters were analyzed using confocal microscopy, while the XRF analyses were performed to evaluate the composition of the bronze coatings. Based on the wettability measurements using oil and water, it was possible to assess that the porous surface acted as oil reservoirs that could prolong the life of lubricating oil layer, and may have resulted in a superior wear resistance. Furthermore, a relevant hydrophobicity was highlighted, suggesting that the surface texturing promoted the water-repellent barrier action on the surface. The experimental results showed that the discrepancy in surface properties in oil and water was raised when using the lead bronze coating. These coupled oleophilic and hydrophobic behaviors could play a beneficial role in sustaining the durability of a lubricating oil layer under a condition of continuous water-droplet impact.

Keywords: wettability; lubrification; oleophilicity; hydrophobicity; laser surface texturing

1. Introduction

Friction and wear processes are generated in all parts subjected to a sliding contact. The study of the tribological behavior of systems in reciprocating contact is a topic of fundamental importance in many industrial fields, such as mechanics [1–3], hydraulics [4], and prosthetics [5,6], in order to reduce the deterioration of components and improve their working life. Ruggiero et al. [7] investigated the tribological performances of tooth-to-tooth contact and material-to-natural tooth contact (zirconia vs. zirconia and natural tooth vs. zirconia) using a reciprocating tribometer under lubricated conditions (artificial saliva). Wang et al. [8] analyzed the effects of textured surfaces on the friction performance of a low-speed and high-torque water hydraulic motor. The experimental results showed that about 62.6% of the wear-loss reduction could be reached using an ellipsoidal pit surface, and the wear loss mainly occurred on the edges of pits.

Typically, the problem of friction and wear is addressed by using lubricants, but in some working conditions, the lubrication may be insufficient. For this reason, in the last few decades, different types of coatings have been studied to guarantee lubrication even in the most severe conditions, such as coatings based on solid lubricants (lead and bismuth) [9,10], functionalized surfaces to create superhydrophobic/superoleophobic coatings [11,12], self-lubricating multilayered coatings [13], or textured surfaces. Surface texturing has been known for a long time, as shown by the numerous studies reported in the scientific literature [14–17], but the aim of this study was to evaluate how the surface texturing affected

the oleophilic and hydrophobic properties of the coating. Yang et al. [18] studied the effects of micro/nano hierarchical structures on the surface of a titanium alloy (Ti-6Al-4V), and observed that the contact angle of the drop increased as the density of the microtextured surface increased, and the wetting state of the textured surfaces conformed to the Cassie model. Volpe et al. [19] analyzed the effects of three different surface-texture geometries on aluminum alloy surfaces. It was shown that by improving the laser texture strategy, it was possible to reduce the laser processing time to produce superhydrophobic surfaces.

In recent times, several surface-texturing techniques have been developed, including micromilling [20], hot embossing [21], electrochemical machining [22], wire EDM machining [23], and surface laser texturing [24–27], which is the most applied technique for obtaining various micropatterns on a material surface due to its high precision, lower environmental impact, good controllability, and flexibility without any chemical treatment. The most widely used surface laser texturing taxonomies include the nanosecond (ns), picosecond (ps), and femtosecond (fs), as they have better controllability, accuracy, and complexity [28]. Due to these advantages, the surface laser texturing technique has been extensively used in numerous applications to improve the tribological performance of coatings, such as lubrication in bearing applications; to improve adhesion bond strength in various coating applications; and fabrication of structures for hydrophobic/superhydrophobic surfaces [29–31].

The laser surface texturing has several advantages in terms of tribo-mechanical behavior. Indeed, the presence of micro-dimples, could allow an enhancement of the tribological behavior optimizing the surface lubrication, thanks to a reservoir action supplied by the tailored surface dimples [32]. Besides, in hydrodynamic or mixed lubrication, these surface microcavities acts as hydrodynamic bearings [33]. A further relevant feature of the laser surface texturing is the capacity to decrease the abrasive wear, since the cavities of the profile behave like trap for the debris that are formed during the relative motions with other bodies improving the tribological properties of the coated surface [27].

Although the tribological behavior of textured coatings has been analyzed in many scientific studies, the focus of the authors is not to evaluate the effect of the texture on the friction and wear of the coating, but rather how the wettability of the coating varies and in particular the hydrophobicity and oleophilic, and therefore lubrication, changing the geometric parameters of the dimples and the composition of the bronze alloy.

The possibility of correlating the microstructural properties with the surface interaction with polar and non-polar liquids, such as water and oil, represents an increase in knowledge for this class of materials, providing further stimuli for their development and industrial applicability of this technique in this field [34,35].

In this paper the wettability measurements with pump oil and water were performed on different types of lead/lead-free textured coating, varying the diameter and density of the dimples. The surface and dimples parameters were analyzed using confocal microscopy, while XRF analyses were performed to evaluate the composition of the bronze coatings.

2. Materials and Methods

2.1. Materials

All tests were carried out on two different bronze alloys (the specimens are shown in Figure 1): one called EN CC480K, which did not contain lead; and one called EN CC496K, with a percentage of lead of about 12%.

These materials are typically used for antifriction coatings in hydraulic pumps and motors, such as on valve plates [36], cylinder blocks [4], and slippers [30], or in the automotive field [37,38]. As is known, in the bronze alloys used for components that can work in conditions of starved lubrication and high friction, lead is used as a solid lubricant. However, lead is a toxic element, and therefore manufacturers are attempting to eliminate or replace it (with bismuth). For the above reasons, we decided to evaluate the behavior of two bronze alloys, one containing lead and one free of lead.

(**a**)   (**b**)
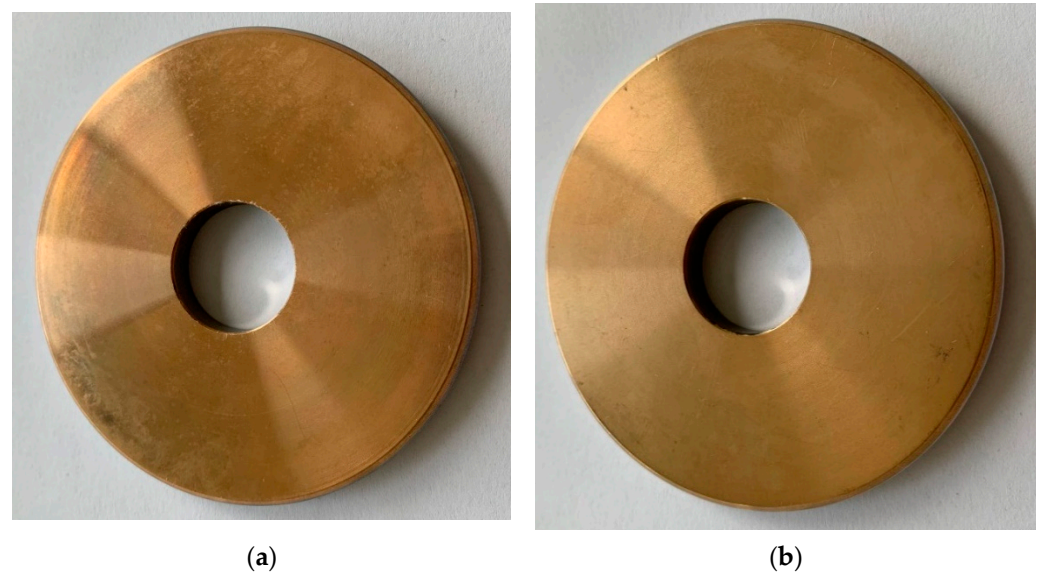
Figure 1. (**a**) EN CC480K bimetal disk (lead-free bronze); (**b**) EN CC496K bimetal disk.

Table 1 shows the results of the XRF analyses of the two different bronze alloys. As shown in the table, the EN CC480K alloy contained 90% copper and a trace amount of Pb, while the EN CC496 K alloy had a high lead content, ranging between 10% and 15%. The effects of the different compositions on the wettabilities of the coatings were analyzed through the use of an EDS analysis.

Table 1. Compositions of bronze alloys.

Bronze Alloys	Sn%	Pb%	Ni%	Si%	Cu%
EN CC480K	7.94	0.06	1.08	0.31	90.5
EN CC496K	10.86	12.43	0.03	0.15	76

The textured microstructures on the bimetal coated cylinder disk samples were obtained by using a surface laser texturing technique (Laser P 400, GF Machining Solution, Schaffhausen, Switzerland), with maximum power of 40 W and a spot size of 15 μm. In particular, the surface texture was tailored by varying the diameter and the density of the dimples on the surface, for both the lead-based and lead-free bronze coatings. The codes and surface-texture parameters for all batches are reported in Table 2.

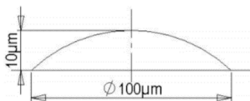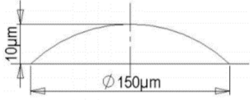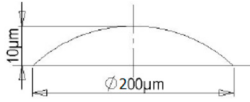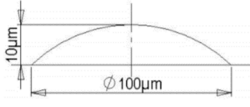**Table 2.** Codes and surface-texture parameters for all batches.
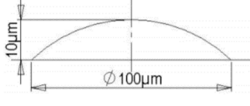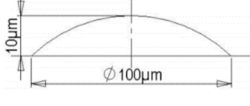
Sample	Typology of Texture	Dimple Diameter (μm)	Density Area (%)
AR	As received	/	/
B100-D10	⌀ 100μm	100	10
B150-D10	⌀ 150μm	150	10
B200-D10	⌀ 200μm	200	10

Table 2. *Cont.*

Sample	Typology of Texture	Dimple Diameter (μm)	Density Area (%)
B100-D20	10μm Ø 100μm	100	20
B100-D30	10μm Ø 100μm	100	30
B100-D40	10μm Ø 100μm	100	40

Samples were investigated with three laser-beam diameters (100, 150, and 200 μm). Furthermore, for a laser beam of 100 μm, four dimple surface densities were analyzed, in the range of 10–40%. For each batch, 3 replicas were created.

A total of 42 samples were created: they were classified based on their textured surface and coating characteristics. In particular, each batch was coded with an acronym using a prefix that referred to the coating characteristic (PbB and PbF, for the Pb-based and Pb-free surfaces, respectively. A second suffix, "B" coupled with a number, referred to the beam diameter (expressed in microns). The last suffix, "C" coupled with a number, referred to the density of the surface area of the laser-melted surface. As an example, the code PbF-B100-D20 indicates a sample with a Pb-free surface, textured with a beam diameter of 100 μm and a surface density of 20%. PbB-AR and PbF-AR codes were used for the as-received samples of Pb-based and Pb-free surfaces, respectively.

2.2. Wettability Measurments

Water-contact-angle measurements were performed by using a tensiometer instrument (AttensionTheta by Biolin Scientific, Gothenburg, Sweden). The test was performed with bidistilled water and pump oil. The oil lubricant used was LI-HIV 46 (viscosity index 175). It is commonly applied in pumps and motors. Table 3 summarizes the main physical parameters of the lubricating oil.

Table 3. LI-HIV 46 oil parameters.

Parameters	Value
Density at 20 °C	873 kg/m^3
Viscosity at 40 °C	46 cSt
Viscosity at 100 °C	9 cSt
Viscosity index	175
Freezing °C	−35
Flammability °C	210

A droplet of the liquid (volume of 3 μL) was softly sited on the coating surfaces in conditions that were open to air and at room temperature (25 °C). After the deposition, the droplet profile was recorded by a microcamera and automatically analyzed by the software supplied with the tensiometer instrument. For each sample, 10 replicas (randomly located on the surface) were performed for all batches.

Morphological analyses of the textured surface and related surface features were carried out by means a 3D confocal optical microscope (Leica DCM 3D, Wetzlar, Germany).

3. Results and Discussion

3.1. Surface Morphology

To better evaluate the surface characteristics of the coatings and the geometry of the dimples, confocal microscopies were carried out on both the EN CC480K alloy coating and the EN CC496K alloy coating. Figure 2 shows the 3D scans of the AR samples (Figure 2a,b) and those of two B150-D10 textured samples (Figure 2c,d). As reported in Table 4, the surface of the PbB-AR sample had a higher average roughness than the PbF-AR sample, measuring approximately 100 nm. This may have been because lead bronze alloys exploit the insolubility of lead in copper to create lead-free globules in a copper–tin matrix. The soft lead phase deformed easily and was smeared on the surface to form a solid lubricant, leaving empty pockets that could have been the cause of the increased roughness.
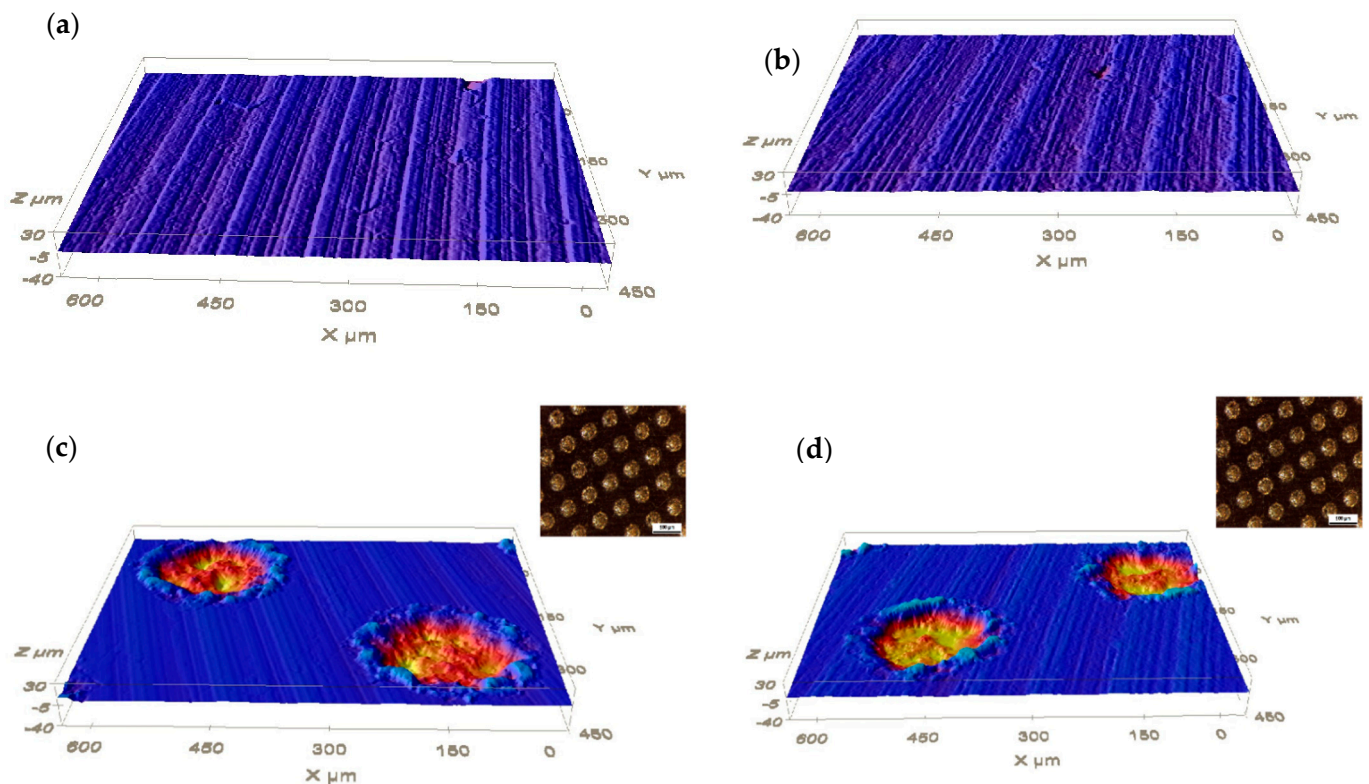
**Figure 2.** Comparison of 3D confocal microscopies: (**a**) PbF-AR sample; (**b**) PbB-AR sample; (**c**) PbF-B150-D10; (**d**) PbB-B150-D10.

Table 4. Roughness parameters of untextured specimens in an area of 636.61×477.25 (μm^2).

| Roughness	PbB-AR	PbF-AR
Max (μm)	1.728	2.495
Min (μm)	−6.220	−6.181
Mean (nm)	474.79	583.25

As shown in Figure 2c,d, the dimensions of the dimples were comparable with the project dimension, although the surface laser texturing technique did not allow them to have a perfect hemisphere. However, it should be noted that the surface laser texturing process caused asperities called pile-ups, which increased the surface roughness by involving an increase in friction and possible debris formation [27,39].

To evaluate the effects of the surface laser texturing on the surface of the bronze coatings, the roughness profiles of the textured samples obtained by varying the diameter of the dimples (Figure 3) and the profiles of the textured samples obtained by varying the

density of the dimples were compared (Figure 4). The roughness profiles were obtained while taking into consideration the portion of the specimen with the maximum density of dimples. When examining the graphs in Figure 3, it is possible to notice some of the negative aspects related to the laser beam texturing technique. In fact, by increasing the diameter of the dimples, the depth of the dimples also increased, reaching peaks of 30 μm (Figure 3c). This was due to the inability of the diameter of the laser beam to draw a perfect hemisphere. Furthermore, as shown in Table 5, as the diameter of the dimples increased, the average surface roughness also increased. This aspect was probably due to the formation of pile-ups (more visible in Figure 3a), which were much greater than the quantity of material removed.

(**a**)

(**b**)

(**c**)
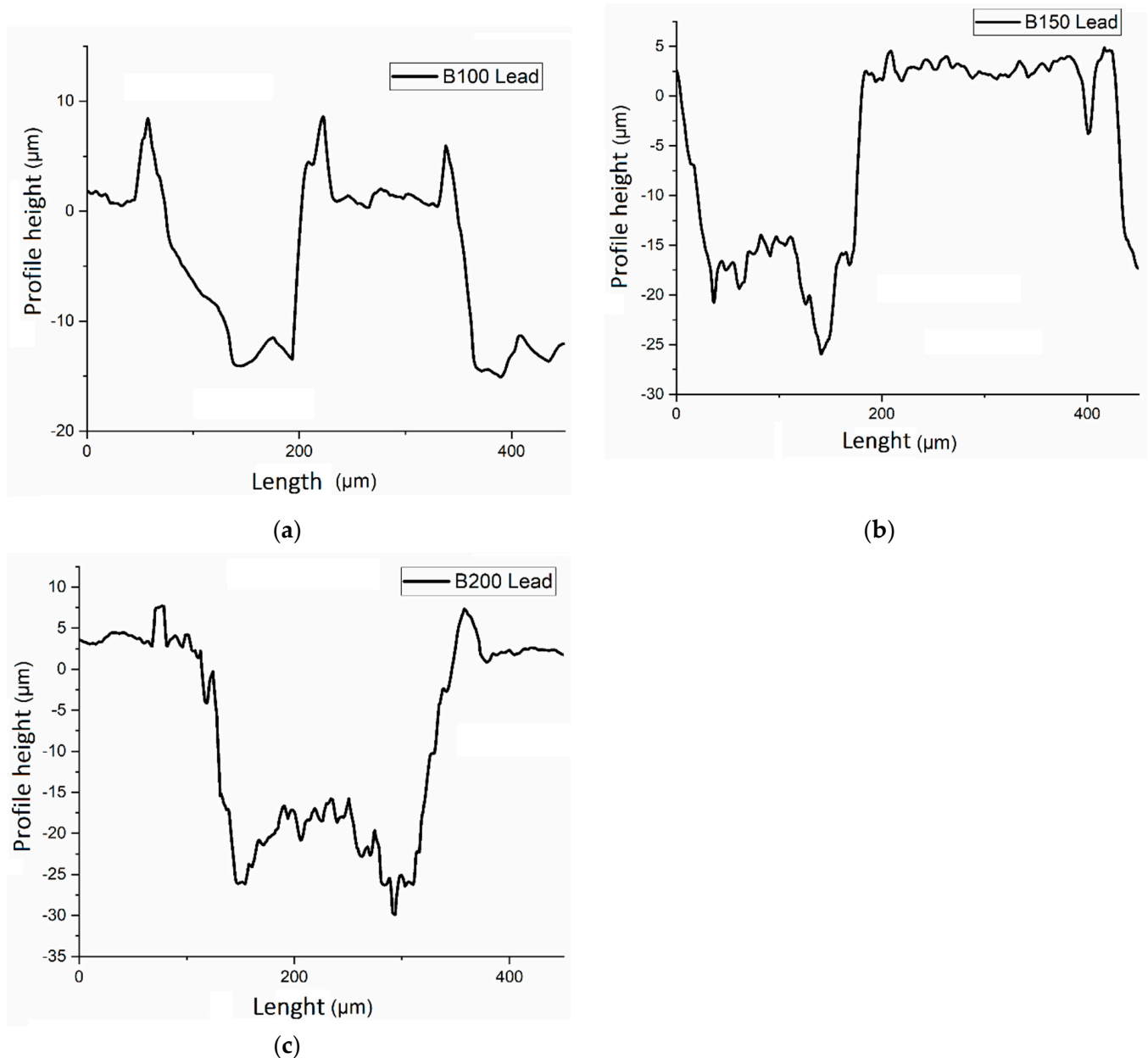
Figure 3. Comparison of roughness profiles when varying dimple diameter: (**a**) PbB-B100-D10; (**b**) PbB-B150-D10; (**c**) PbB-B200-D10.

(a)

(b)

(c)
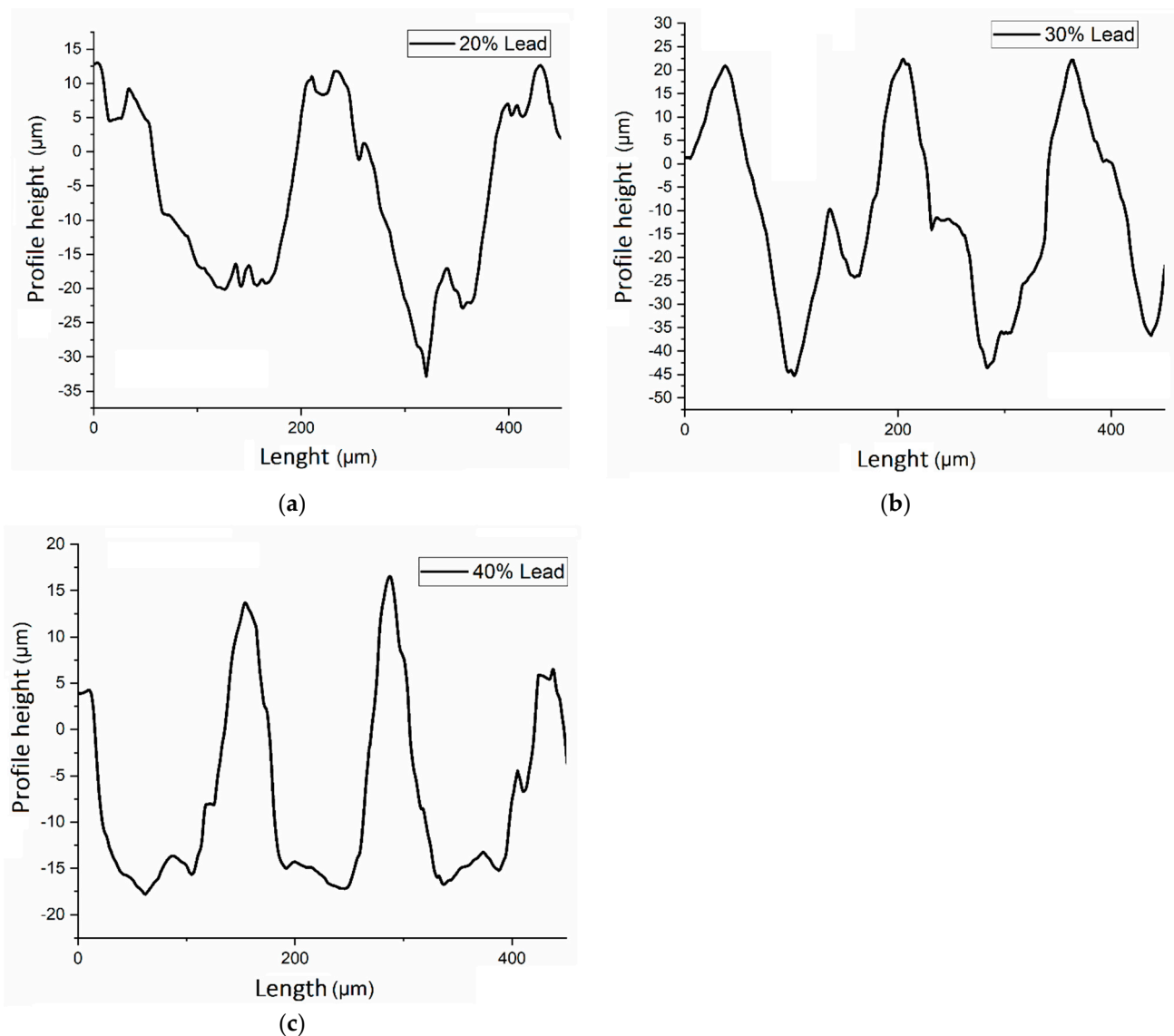
Figure 4. Comparison of roughness profiles when varying dimple density: (**a**) PbB-B100-D20; (**b**) PbB-B100-D30; (**c**) PbB-B100-D40.

Table 5. Roughness parameters of PbB specimens with different dimple diameters in an area of 636.61×477.25 (μm^2).

| Roughness	PbB-B100-D10	PbB-B150-D10	PbB-B200-D10
Max (μm)	17.409	11.174	8.866
Min (μm)	−16.384	−31.646	−34.295
Mean (μm)	3.330	4.161	4.584

Figure 4 shows a comparison of the roughness profiles as the density varied. What should be noted when analyzing the curves is that the greater the density of the dimples on the surface, the smaller the portion of material that separated one dimple from another, until it became real roughness in the case of the PbB-B100-D40 sample. While the increase in the density of the dimples ensured a more effective lubrication due to the greater presence of "oil reservoirs" on the surface, on the other hand, it also involved a substantial increase in the surface roughness, approximately 3–4 times greater than that obtained by varying the diameter of the dimples. Furthermore, as shown in Table 6, in this case the depth values for the dimples that were obtained were even higher than in the previous case, up to 40–45 μm

in depth. However, as will be analyzed in the next chapter, a greater increase in roughness led to an increase in the hydrophobic characteristics of the coatings.

Table 6. Roughness parameters of PbB specimens with different dimple densities in an area of 636.61×477.25 (μm^2).

Roughness	PbB-B100-D20	PbB-B100-D30	PbB-B100-D40
Max (μm)	14.472	28.936	27.515
Min (μm)	−45.045	−49.443	−18.330
Mean (μm)	8.1984	12.579	10.467

Figure 5 shows a comparison of the roughness profiles of the lead-free bronze and lead bronze samples. As shown in Figure 5a,b, in the cases of both the PbB-B100-D10 and PbB-B100-D40 samples, the profile drawn by the dimples had a more regular trend, and the lower surface of the dimples had a less-indented appearance. This more regular trend was justified by the lower hardness of the lead bronze coating compared to the free-lead bronze. In fact, for both the PbF-B100-D10 and PbB-B100-D40 samples, the depths of the dimples were much greater than that defined in Table 2, and this was justified by the longer time taken by the laser to melt the coating.

(**a**)   (**b**)
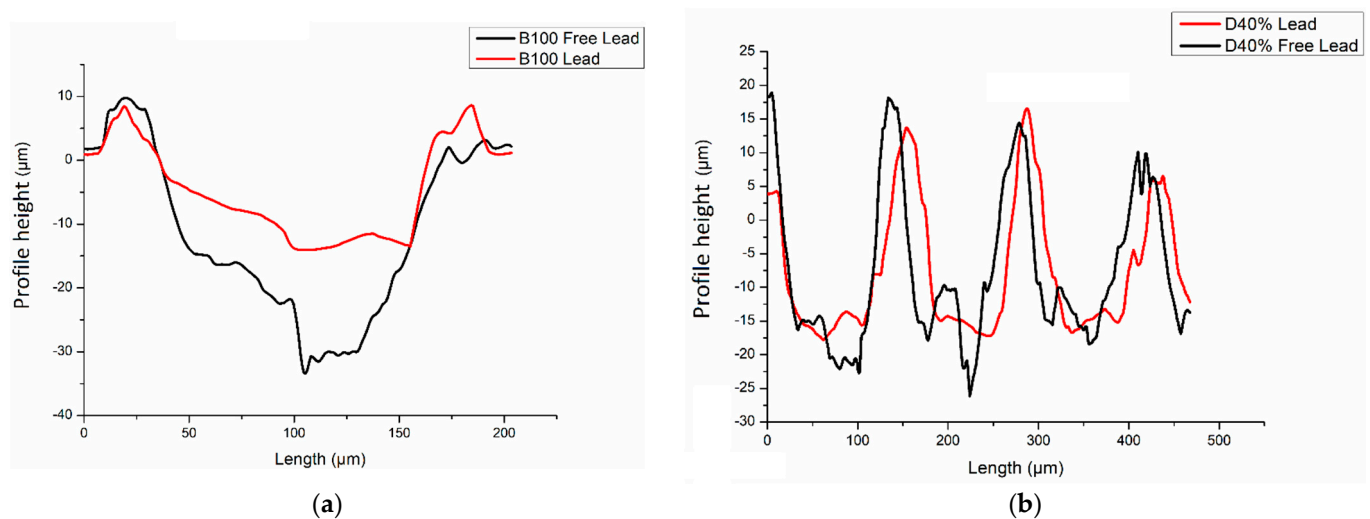
Figure 5. (**a**) Comparison of the roughness profiles of the PbB-B100-D10 and PbF-B100-D10 samples; (**b**) comparison of the roughness profiles of the PbB-B100-D40 and PbF-B100-D40 samples.

Figure 6 shows the statistical parameters of the surface profile used to analyze the correspondence between the geometric design parameters of the texture and the real geometric parameters averaged as a function of 10 measurements for each type of texture. Therefore, by analyzing the statistical parameters of the texture, the numerical values of which are shown in Table 7, it was possible to confirm that the surface laser texturing process generated a variability of a few tens of microns with respect to the design values, and this was due to the diameter of the laser beam of the machine used, as well as the type of material. It is important to specify that the data were obtained while considering both the PbF and PbB specimens to have broader statistical data. However, as already mentioned, and as shown in Figure 5, there was a difference in workability between the two types of coatings that certainly depended on the presence of lead.
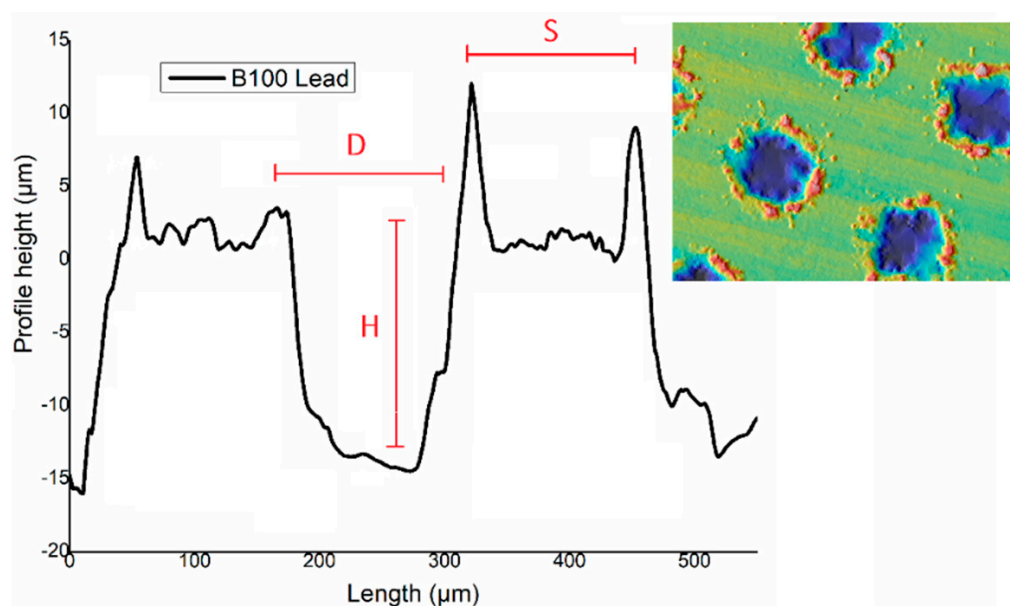
Figure 6. Representation of the geometric parameters used for statistical analysis.

Table 7. Variation of surface geometric parameters.

| Parameters	B100-D10	B150-D10	B200-D10	B100-D20	B100-D30	B100-D40
S (µm)	119.50 ± 8	243 ± 20	411 ± 22	38.2 ± 5	16 ± 6	15.7 ± 2
D (µm)	113 ± 10	165.4 ± 15	221.6 ± 20	119.2 ± 7	138 ± 8	154.3 ± 4
H (µm)	14.1 ± 3	22.7 ± 5	27 ± 2	26.4 ± 7	37.3 ± 10	20.4 ± 4

3.2. Surface Wettability

In order to better correlate the morphologies of the textured surfaces with the surface properties of the bronze coatings, wettability measurements were carried out. Some representative images of 3 mL droplets deposited on the textured surfaces, with varying surface texturing, are shown in Figures 7 and 8 for both the Pb-based and Pb-free coated surfaces. In particular, the wettability measurements were carried out with water (polar liquid—Figure 7) and pumping oil (nonpolar liquid 002D—Figure 8).
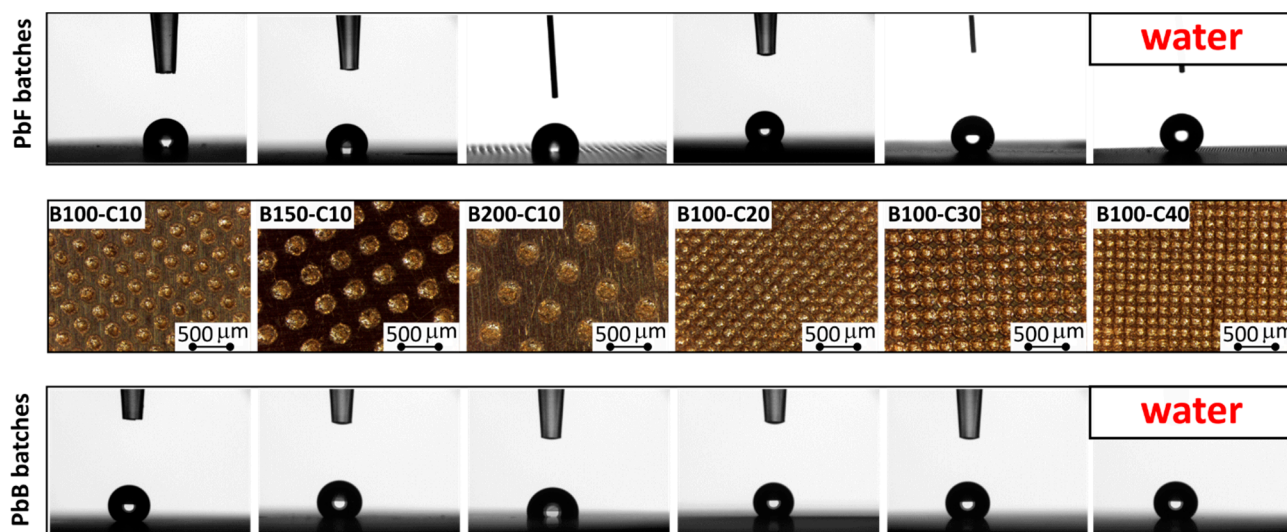
Figure 7. Water droplets for all Pb-based and Pb-free textured surfaces.
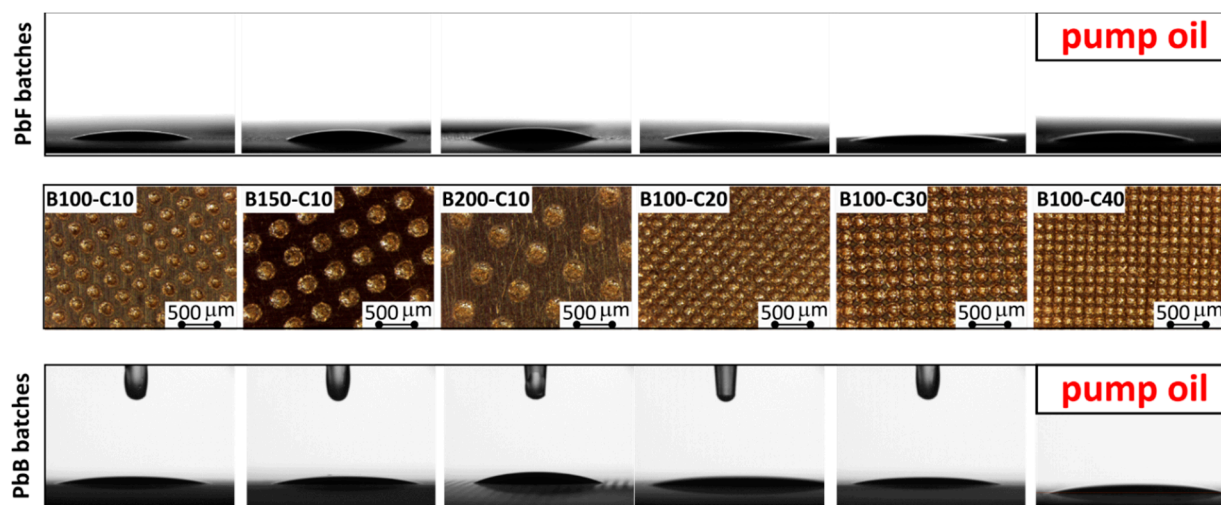
Figure 8. Oil droplets for all Pb-based and Pb-free textured surfaces.

When evaluating the wettability results, an evident correlation of the surface properties with the polar and nonpolar characteristics of the liquid was identified. All the specimens in both the PbB and PbF batches showed a predominantly hydrophobic behavior with water and an oleophilic one with pump oil. In particular, the surfaces showed a strong interaction with the oil, which spread easily in the interstices of the textured surface, which led to very low contact angles.

Moreover, it is worth noting that the texturing procedure contributed significantly to modifying the surface properties of the bronze coatings. The PbB-AR and PbF-AR specimens showed a more evident surface hydrophilicity and a less marked oleophilic one compared to the surface-treated ones. This qualitatively suggested that the surface without laser treatment did not allow selective operation toward liquids, potentially offering a less-effective lubricating capacity.

In order to be able to better quantitatively correlate the surface wettability performances with the surface morphologies, Table 8 summarizes the water contact angle (WCA) and pump oil contact angle (OCA) for all the investigated batches.

Table 8. Water and pump oil contact angles for PbF and PbB batches.

PbF Batches	WCA (°)	OCA (°)	PbB Batches	WCA (°)	OCA (°)
PbF-AR	93.0 ± 3.7	16.5 ± 1.6	PbB-AR	100.0 ± 3.7	29.3 ± 2.9
PbF-B100-D10	109.6 ± 3.6	17.2 ± 1.7	PbB-B100-D10	149.9 ± 4.2	12.2 ± 1.2
PbF-B150-D10	122.1 ± 3.2	20.2 ± 2.0	PbB-B150-D10	133.5 ± 4.8	11.6 ± 1.2
PbF-B200-D10	100.1 ± 2.5	20.1 ± 2.0	PbB-B200-D10	105.3 ± 4.0	22.0 ± 2.2
PbF-B100-D20	134.9 ± 7.0	14.0 ± 1.4	PbB-B100-D20	140.8 ± 3.6	10.5 ± 1.0
PbF-B100-D30	149.5 ± 4.2	9.3 ± 0.9	PbB-B100-D30	141.5 ± 2.1	11.2 ± 1.1
PbF-B100-D40	144.3 ± 4.8	15.6 ± 1.6	PbB-B100-D40	145.5 ± 3.0	13.0 ± 1.3

Concerning the PbF batch, the laser surface texturing induced an increase in the contact angle in a range of about 15°–50°. The higher result was observed for PbF-B100-D30, which showed a WCA of 149.5°, close to the superhydrophobic threshold [31].

When evaluating the evolution of the WCA values with varied surface texturing, it was seen that the dimple size played a less-relevant role than the dimple density. Indeed, the specimens characterized by the same density and a growing dimple size showed slight similar water contact angle values. Conversely, with increasing dimple density, a significant increase in the hydrophobic surface properties occurred.

In addition, when assessing the evolution of the OCA trend when varying the surface texturing, the oleophilic properties were quite similar, if not worse. Only the PbF-B100-D30

batch showed an evident increase in the interfacial affinity with nonpolar liquids, as shown by an average OCA value of 9.3°.

Different considerations could be addressed by evaluating the contact angle values for the PbB batches. For samples with the lead-based bronze coating, the laser surface texturing had an evident effect on the surface wettability performances. A coupled increase in the hydrophobic and oleophilic behaviors took place. All samples characterized by a laser beam diameter of 100 μm exhibited a WCA close to 150°. Furthermore, the OCA experienced a reduction of up to 20°.

Not only the liquid/solid contact angles were evaluated, but also the sliding angles, in order to understand the surface wettability behavior [40]. All the samples before and after texturing showed a high liquid sliding angle (90°), indicating a high liquid adhesion (data not reported in the table). Thus, creating a textured structure did not change the water adhesion on the sample surface, regardless of the coating nature.

The marked hydrophobic and oleophilic behaviors found in the laser-textured samples could be related to the intrinsic surface morphology acquired by the coatings at the end of the surface treatment. The resulting surface profile was constituted by a larger number of peaks and valleys, making the surface regularly jagged and rough.

This was in accordance with Wenzel's theory, which relates the surface roughness to the liquid/solid contact angle [41,42]. Indeed, Wenzel proposed a relationship between the surface-roughness ratio (*R*: ratio of the rough surface area to the smooth surface one) and the contact angles on smooth and rough surfaces:

$$cos(\theta w) = R \ cos(\theta) \tag{1}$$

where θw is the Wenzel contact angle (contact angle on rough surface) and θ is the ideal contact angle (contact angle on smooth surface). According to this equation, by increasing the surface roughness, the hydrophobic surface becomes more hydrophobic, and the hydrophilic surface becomes more hydrophilic [43]. In fact, as shown in Table 4, both PbR_AR and PbB-AR were hydrophobic and oleophilic before texturing, and they become more hydrophobic and oleophilic after texturing. In this Wenzel state, the liquid penetrated the rough surface cavities; such behavior is known as the homogenous wetting mode, in which the interaction and the adhesion between the liquid and the solid surface are high [44].

In order to better investigate the correlation between the wettability and the characteristics of the surface profile of the specimens, an index related to the dimples' surface morphologies, named the DS index, was calculated according to the following expression:

$$DS \ index = (d * h)/s \tag{2}$$

where *d* and *h* are the diameter and height of the dimple, respectively. Consequently, $d * h$ is the dimple area, and *S* is the length of the peak between two dimples. All the measurements were defined in μm, thus the DS index was expressed in μm. The greater this index, the greater the contribution of the cavities to the surface peaks.

Figure 9 shows the evolution of the water contact angle (WCA) and oil contact angle (OCA) with the DS index for Pb-based and Pb-free textured samples.

For PbF batches (blue diamond marker in Figure 9), the WCA and OCA had a quite good linear relationship with the DS index. The slope increased for the WCA values, and vice versa (the slope decreased for the OCA). This result suggested that an increase in the size of the dimples and their depth played a key role in enhancing the hydrophobic and oleophilic behavior of the surface.

For the PbB batches (orange circle marker in Figure 9), a clear bilinear trend in the WCA and OCA vs. DS index could instead be identified. The trend initially showed a strong change in the contact angles due to a slight change in the DS index. The slope of the fitting line (positive for WCA and negative for OCA) was very high. Subsequently, for values of DS > 1.4, the trend showed a plateau zone. An increase in the dimple shape

(diameter and depth) did not provide a statistically significant change in the contact angle. The fitting line had a very low slope, indicating a trend almost parallel to the *x* axis.

(**a**)

(**b**)
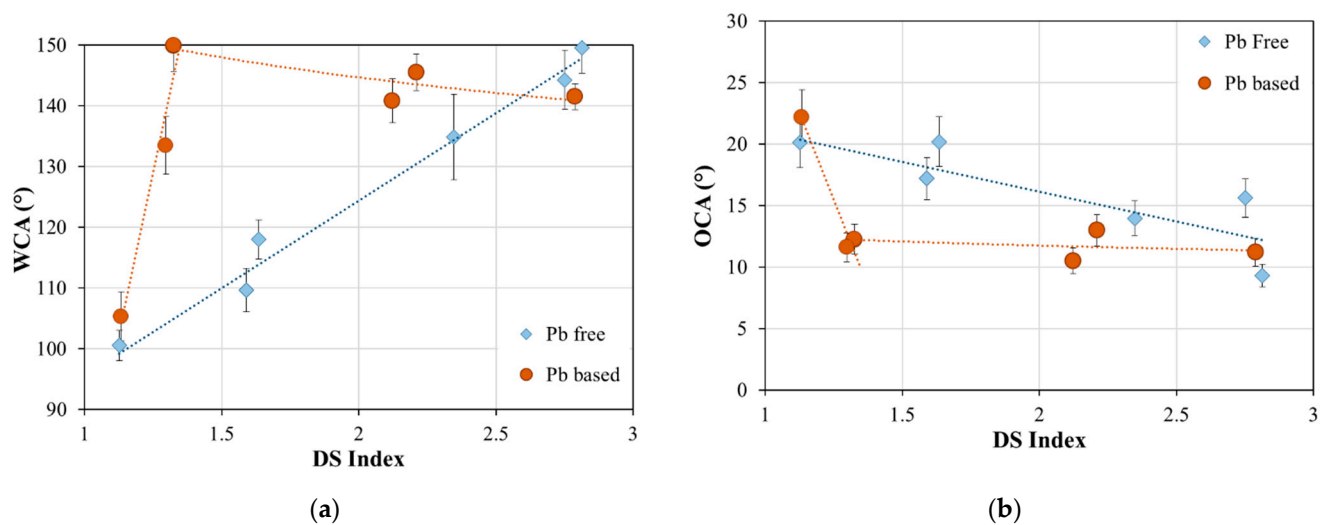
Figure 9. Evolution of (**a**) water contact angle (WCA) and (**b**) oil contact angle (OCA) with the DS index for Pb-based and Pb-free textured samples.

This behavior showed that for the PbB batch, a very extensive and invasive laser texturing was not necessary to induce a surface-modification effect in the coating. A DS index close to 4 was sufficient to guarantee an effective surface hydrophilicity and hydrophobicity.

Based on wettability measurements with oil and water, it was possible to assess that the porous textured surface was tailored to act an oil reservoir thanks to its good oleophilic behavior. This can prolong the life of lubricating oil layer and may result in a superior wear resistance. Furthermore, a relevant hydrophobicity was highlighted, suggesting that the surface texturing promoted the water-repellent barrier action on the surface.

4. Conclusions

The experimental studies in this paper were conducted to understand the influence of surface laser texturing and roughness on the wettability of lead-free bronze and lead bronze coatings. In order to increase the efficiency of components that work under reciprocating sliding, classes of textured specimens were obtained by varying the diameter of the dimples in a range of values between 100 and 200 μm and varying the surface density of the dimples between 10 and 40%. By using a low-economic-impact technique, such as surface laser texturing, it is possible to decrease the friction coefficient by increasing the hydrophobicity and oleophilic, and therefore improve lubrication, especially in lubrication-starved conditions. The results obtained on the basis of the wettability measurements with oil and water highlighted that the porous textured surface was adapted to serve as an oil reservoir thanks to its good oleophilic behavior. This can extend the life of the lubricating oil layer and ensure better lubrication, even in hard-working conditions, resulting in superior wear resistance. Furthermore, a significant hydrophobicity was highlighted, suggesting that the surface texturing favored the water-repellent barrier action on the surface. For the tests carried out on the PbF specimens, it was experimentally shown that an increase in the size of the dimples and their depths played a key role in enhancing the hydrophobic and oleophilic behavior of the surface, while regarding the PbB specimens, an increase in the dimple shape (diameter and depth) did not provide a statistically significant change in the contact angle, and therefore it was sufficient to guarantee a DS equal to 4, meaning a coating with good hydrophobicity and oleophilic. Future work will concern the correlation of the wettability tests with the tribological behavior of the coatings (both PbF and PbB) in order to evaluate the extent to which the application of the surface texture affects the friction coefficient of the coatings and the wear rate.

References

1. Tang, Z.; Liu, X.; Liu, K. Effect of surface texture on the frictional properties of grease lubricated spherical plain bearings under reciprocating swing conditions. *Proc. Inst. Mech. Eng. Part J J. Eng. Tribol.* **2017**, *231*, 125–135. [CrossRef]
2. Ali, M.K.A.; Xianjun, H.; Essa, F.A.; Abdelkareem, M.A.A.; Elagouz, A.; Sharshir, S.W. Friction and wear reduction mechanisms of the reciprocating contact interfaces using nanolubricant under different loads and speeds. *J. Tribol.* **2018**, *140*, 051606. [CrossRef]
3. Hua, D.; Wang, W.; Luo, D.; Zhou, Q.; Li, S.; Shi, J.; Fu, M.; Wang, H. Molecular dynamics simulation of the tribological performance of amorphous/amorphous nano-laminates. *J. Mater. Sci. Technol.* **2022**, *105*, 226–236. [CrossRef]
4. D'Andrea, D.; Epasto, G.; Bonanno, A.; Guglielmino, E.; Benazzi, G. Failure analysis of anti-friction coating for cylinder blocks in axial piston pumps. *Eng. Fail. Anal.* **2019**, *104*, 126–138. [CrossRef]
5. Liu, X.; Tang, J.; Li, X.; Li, W. Study on friction behavior at the interface between prosthetic socket and liner. *Acta Bioeng. Biomech.* **2021**, *23*, 83–93. [CrossRef]
6. D'Andrea, D.; Pistone, A.; Risitano, G.; Santonocito, D.; Scappaticci, L.; Alberti, F. Tribological characterization of a hip prosthesis in Si3N4-TiN ceramic composite made with Electrical Discharge Machining (EDM). *Procedia Struct. Integr.* **2021**, *33*, 469–481. [CrossRef]
7. Ruggiero, A.; D'Amato, R.; Sbordone, L.; Haro, F.B.; Lanza, A. Experimental comparison on dental BioTribological pairs zirconia/zirconia and zirconia/natural tooth by using a reciprocating tribometer. *J. Med. Syst.* **2019**, *43*, 97. [CrossRef]
8. Wang, Z.; Xiang, J.; Fu, Q.; Wood, R.J.K.; Wang, S. Study on the friction performance of textured surface on water hydraulic motor piston pair. *Tribol. Trans.* **2022**, *65*, 308–320. [CrossRef]
9. Yang, D.; Li, W.; Wang, H.; Gao, G.; Cheng, S.; Ren, J.; Tian, S. Effect of Counterpart Ring Surface Roughness on Wear Process of Bismuth Bronze. *Chin. J. Mater. Res.* **2021**, *35*, 732–740.
10. Kestursatya, M.; Kim, J.K.; Rohatgi, P.K. Wear performance of copper-graphite composite and a leaded copper alloy. *Mater. Sci. Eng. A* **2003**, *339*, 150–158. [CrossRef]
11. Dyett, B.; Lamb, R. Correlating Material Properties with the Wear Behavior of Sol–Gel Derived Superhydrophobic Films. *Adv. Mater. Interfaces* **2016**, *3*, 1500680. [CrossRef]
12. Calabrese, L.; Khaskhoussi, A.; Patane, S.; Proverbio, E. Assessment of Super-Hydrophobic Textured Coatings on AA6082 Aluminum Alloy. *Coatings* **2019**, *9*, 352. [CrossRef]
13. Luo, D.; Zhou, Q.; Ye, W.; Ren, Y.; Greiner, C.; He, Y.; Wang, H. Design and Characterization of Self-Lubricating Refractory High Entropy Alloy-Based Multilayered Films. *ACS Appl. Mater. Interfaces* **2021**, *13*, 55712–55725. [CrossRef] [PubMed]
14. Kovalchenko, A.; Ajayi, O.; Erdemir, A.; Fenske, G.; Etsion, I. The effect of laser texturing of steel surfaces and speed-load parameters on the transition of lubrication regime from boundary to hydrodynamic. *Tribol. Trans.* **2004**, *47*, 299–307. [CrossRef]
15. Etsion, I. Improving tribological performance of mechanical components by laser surface texturing. *Tribol. Lett.* **2004**, *17*, 733–737. [CrossRef]
16. Etsion, I.; Halperin, G. A laser surface textured hydrostatic mechanical seal. *Seal. Technol.* **2003**, *45*, 430–434. [CrossRef]
17. Shum, P.W.; Zhou, Z.F.; Li, K.Y. Investigation of the tribological properties of the different textured DLC coatings under reciprocating lubricated conditions. *Tribol. Int.* **2013**, *65*, 259–264. [CrossRef]
18. Yang, Z.; Zhu, C.; Zheng, N.; Le, D.; Zhou, J. Superhydrophobic surface preparation and wettability transition of titanium alloy with micro/nano hierarchical texture. *Materials* **2018**, *11*, 2210. [CrossRef]
19. Volpe, A.; Covella, S.; Gaudiuso, C.; Ancona, A. Improving the laser texture strategy to get superhydrophobic aluminum alloy surfaces. *Coatings* **2021**, *11*, 369. [CrossRef]
20. Chen, L.; Liu, Z.; Shen, Q. Enhancing tribological performance by anodizing micro-textured surfaces with nano-MoS2 coatings prepared on aluminum-silicon alloys. *Tribol. Int.* **2018**, *122*, 84–95. [CrossRef]

21. Gao, P.; Liang, Z.; Wang, X.; Zhou, T.; Xie, J.; Li, S.; Shen, W. Fabrication of a micro-lens array mold by micro ball end-milling and its hot embossing. *Micromachines* **2018**, *9*, 96. [CrossRef] [PubMed]

22. Chen, X.L.; Dong, B.Y.; Zhang, C.Y.; Wu, M.; Guo, Z.N. Jet electrochemical machining of micro dimples with conductive mask. *J. Mater. Process. Technol.* **2018**, *257*, 101–111. [CrossRef]

23. Holmberg, J.; Berglund, J.; Wretland, A.; Beno, T. Evaluation of surface integrity after high energy machining with EDM, laser beam machining and abrasive water jet machining of alloy 718. *Int. J. Adv. Manuf. Technol.* **2019**, *100*, 1575–1591. [CrossRef]

24. Despres, L.; Costil, S.; Cormier, J.; Villechaise, P.; Cariou, R. Impact of Laser Texturing on Ni-Based Single Crystal Superalloys. *Metals* **2021**, *11*, 1737. [CrossRef]

25. Conradi, M.; Kocijan, A.; Klobčar, D.; Godec, M. Influence of laser texturing on microstructure, surface and corrosion properties of Ti-6Al-4V. *Metals* **2020**, *10*, 1504. [CrossRef]

26. Travessa, D.N.; Guedes, G.V.B.; de Oliveira, A.C.; Cardoso, K.R.; Roche, V.; Jorge, A.M., Jr. The effect of surface laser texturing on the corrosion performance of the biocompatible β-Ti12Mo6Zr2Fe alloy. *Surf. Coat. Technol.* **2021**, *405*, 126628. [CrossRef]

27. Senatore, A.; Risitano, G.; Scappaticci, L.; D'andrea, D. Investigation of the tribological properties of different textured lead bronze coatings under severe load conditions. *Lubricants* **2021**, *9*, 34. [CrossRef]

28. Rajab, F.H.; Liu, Z.; Li, L. Long term superhydrophobic and hybrid superhydrophobic/superhydrophilic surfaces produced by laser surface micro/nano surface structuring. *Appl. Surf. Sci.* **2019**, *466*, 808–821. [CrossRef]

29. Li, M.; Li, Y.; Xue, F.; Jing, X. A robust and versatile superhydrophobic coating: Wear-resistance study upon sandpaper abrasion. *Appl. Surf. Sci.* **2019**, *480*, 738–748. [CrossRef]

30. Rizzo, G.; Massarotti, G.P.; Bonanno, A.; Paoluzzi, R.; Raimondom, M.; Blosi, M.; Veronesi, F.; Caldarelli, A.; Guarini, G. Axial piston pumps slippers with nanocoated surfaces to reduce friction. *Int. J. Fluid Power* **2015**, *16*, 1–10. [CrossRef]

31. Khaskhoussi, A.; Calabrese, L.; Proverbio, E. An Easy Approach for Obtaining Superhydrophobic Surfaces and their Applications. *Key Eng. Mater.* **2019**, *813*, 37–42. [CrossRef]

32. Rosén, B.-G.; Nilsson, B.; Thomas, T.R.; Wiklund, D.; Xiao, L. Oil pockets and surface topography: Mechanisms of friction reduction. In Proceedings of the XI. International Colloquium on Surfaces, Chemnitz, Germany, 24–28 September 2004.

33. Costa, H.L.; Hutchings, I.M. Hydrodynamic lubrication of textured steel surfaces under reciprocating sliding conditions. *Tribol. Int.* **2007**, *40*, 1227–1238. [CrossRef]

34. Bharatish, A.; Rajkumar, G.R.; Gurav, P.; Satheesh Babu, G.; Narasimha Murthy, H.N.; Roy, M. Optimization of laser texture geometry and resulting functionality of nickel aluminium bronze for landing gear applications. *Int. J. Light. Mater. Manuf.* **2021**, *4*, 346–357. [CrossRef]

35. Li, J.; Liu, S.; Yu, A.; Xiang, S. Effect of laser surface texture on CuSn6 bronze sliding against PTFE material under dry friction. *Tribol. Int.* **2018**, *118*, 37–45. [CrossRef]

36. Wang, Z.; Gu, L.; Li, L. Experimental studies on the overall efficiency performance of axial piston motor with a laser surface textured valve plate. *Proc. Inst. Mech. Eng. Part B J. Eng. Manuf.* **2013**, *227*, 1049–1056. [CrossRef]

37. Ryk, G.; Kligerman, Y.; Etsion, I. Experimental investigation of laser surface texturing for reciprocating automotive components. *Tribol. Trans.* **2002**, *45*, 444–449. [CrossRef]

38. Guarnaccio, A.; Belviso, C.; Montano, P.; Toschi, F.; Orlando, S.; Ciaccio, G.; Ferreri, S.; Trevisan, D.; Mollica, D.; Parisi, G.P.; et al. Femtosecond laser surface texturing of polypropylene copolymer for automotive paint applications. *Surf. Coat. Technol.* **2021**, *406*, 126727. [CrossRef]

39. Kümmel, D.; Hamann-Schroer, M.; Hetzner, H.; Schneider, J. Tribological behavior of nanosecond-laser surface textured Ti6Al4V. *Wear* **2019**, *422*, 261–268. [CrossRef]

40. Khaskhoussi, A.; Calabrese, L.; Proverbio, E. Superhydrophobic Self-Assembled Silane Monolayers on Hierarchical 6082 Aluminum Alloy for Anti-Corrosion Applications. *Appl. Sci.* **2020**, *10*, 2656. [CrossRef]

41. Wenzel, R.N. Resistance of solid surfaces to wetting by water. *Ind. Eng. Chem.* **1936**, *28*, 988–994. [CrossRef]

42. Khaskhoussi, A.; Calabrese, L.; Proverbio, E. Effect of the Cassie Baxter-Wenzel behaviour transitions on the corrosion performances of AA6082 superhydrophobic surfaces. *Metall. Ital.* **2021**, *5*, 15–21.

43. Jiang, G.; Hu, J.; Chen, L. Preparation of a Flexible Superhydrophobic Surface and Its Wetting Mechanism Based on Fractal Theory. *Langmuir* **2020**, *36*, 8435–8443. [CrossRef] [PubMed]

44. Khaskhoussi, A.; Calabrese, L.; Patané, S.; Proverbio, E. Effect of Chemical Surface Texturing on the Superhydrophobic Behavior of Micro-Nano-Roughened AA6082 Surfaces. *Materials* **2021**, *14*, 7161. [CrossRef] [PubMed]